

# Mixing of a starting turbulent jet in homogeneous and isotropic turbulence

Chaoxu Chen\*, Yannis Hardalupas, Alex M.K.P. Taylor

1: Dept. of Mechanical Engineering, Imperial College London, UK

\* Correspondent author: c.chen16@imperial.ac.uk

**Keywords:** Starting jet, Mixing, Mixture fraction, Scalar dissipation rate, Homogeneous and isotropic turbulence, PLIF

## ABSTRACT

The mixing of a starting turbulent jet, injected with an injection velocity  $U = 18.8$  m/s from a tube with a diameter  $D = 4$  mm (Reynolds number  $Re = 4800$ , characteristic time scale  $t^* = D/U = 0.21$  ms at the nozzle exit), was experimentally investigated in the presence of homogenous and isotropic turbulence (HIT) using Planar Laser-induced Fluorescence (PLIF). The root-mean-square (RMS) velocity of the ambient HIT was 0.38 and 0.63 m/s, corresponding to turbulent Reynolds numbers of  $Re_\lambda = 190$  and 250, respectively. Spatial distributions of mixture fraction and scalar dissipation rate (SDR) were measured within an axial range of  $y = 0 - 10 D$  and at different times after the start of injection (ASIs) up to  $21.4 t^*$ . Ambient HIT did not alter the location or size of the leading vortex ring in the initial formation stage. However, it was able to enhance the entrainment of ambient fluids in this stage and deform/transport both the leading and the trailing vortex rings at later stages, despite that the ASIs were only comparable to its Kolmogorov timescale. Ambient HIT also introduced a significant increase to the fluctuations of the jet penetration length but only a marginal reduction (less than 10%) to the averaged jet penetration speed. PDFs of the ensemble averaged mixture fraction within the whole jet region showed an increased probability of low mixture fraction values – and therefore indicating enhanced entrainment and mixing – in the presence of ambient HIT. Ensemble averaged distributions of SDR showed no significant alterations by the ambient HIT in the initial formation stage of the leading vortex ring. At later stages, while the high SDRs in the leading vortex ring remained concentrated in a layer along the boundaries of the vortex ring for  $Re_\lambda = 0$ , they became increasingly uniformly distributed with a lower maximum value as the ambient HIT increased. Similar, but less significant, impact of the ambient HIT on the SDR fields was observed in the trailing vortex rings, while no noticeable impact was found in the shear layer close to the nozzle exit.

---

## 1. Introduction

Turbulent jet is one of the simplest yet ubiquitous types of flow, and has long been the object of turbulent flow studies (e.g., List, 1982; Pope, 2000; Tennekes & Lumley, 1972). Therefore, the understanding of the mixing process of steady state turbulent jets within a quiescent or laminar environment has been well established. In practical applications/manifestations of turbulent jets, jet fluid is often ejected into an environment with existing turbulence; examples include fuel injections in the combustion chambers of gas turbines, and releases of gas and/or liquid into the atmosphere/rivers/lakes/oceans in industrial activities. The impact of the ambient turbulence on

the mixing process of steady state turbulent jets has also been investigated in many studies (e.g., Khorsandi et al., 2013; Perez Alvarado, 2016, and references therein). Khorsandi et al. (2013) and Perez Alvarado (2016) measured the velocity and concentration fields within axisymmetric turbulent jets issued into HIT. They found that ambient turbulence was able to accelerate the decay of the axial velocity and jet fluid concentration and increase the jet spreading rate. However, the entrainment rate of the turbulent jets was reported to reduce in the presence of ambient turbulence (Gaskin et al., 2004; Khorsandi et al., 2013; Sahebjam et al., 2022).

In scenarios such as fuel injection and pre-chamber ignition in internal combustion engines, jet fluids are issued into the ambient turbulence in a short pulse, which therefore entails transient turbulent jets such as in the stage immediately after the start of injection and before the jet reaches the steady state, often referred to as the "starting jets". The development of starting turbulent jets has been extensively investigated in quiescent environment, both experimentally (e.g., Cossali et al., 2001; Johari et al., 1997; Witze, 1980) and numerically (e.g., Iglesias et al., 2005; Inanc et al., 2016). The structure of starting turbulent jets is distinctly different from that of steady-state turbulent jets. One of such differences is the formation of discrete vortex rings with relatively large scales (Krueger & Gharib, 2003; Yu et al., 2007). Wang et al. (2019) recently compared the vorticity fields of a starting turbulent jet and of a steady-state turbulent jet, and concluded that the disappearance of these discrete vortex rings symbolizes the transition of a starting jet into the steady state. Differences in the jet structure between the two states cause differences in the entrainment and mixing process. For example, Iglesias et al. (2005) reported that the leading vortex ring formed in the starting jet entrained mainly jet fluids instead of ambient fluids during the early state of its formation. It was also found that the entrainment rate of ambient fluids near the tip of the trailing jet was much greater than that in the leading vortex ring (Johari et al., 1997).

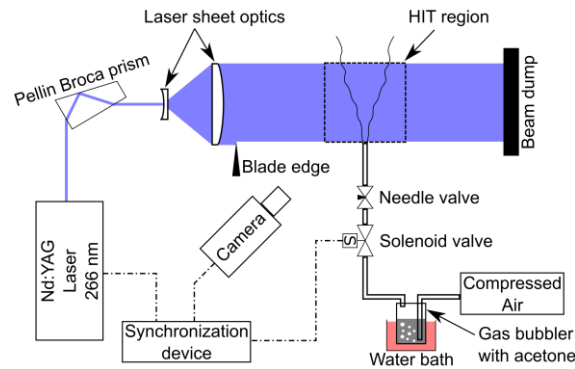
The mixing of starting jets with ambient fluids is critical in applications involving non-premixed combustion, such as the combustion of the fuel jets in internal combustion engines, because chemical reactions can only take place once the jet fluids and the ambient fluids has mixed to an appropriate degree at the molecular level. The degree of mixing is often characterised by mixture fraction ( $\xi$ ), which is a conserved scalar and defined as the fraction of local mixture that originates from the fuel stream (Peters, 2000). Another important parameter in turbulent non-premixed combustion is the scalar dissipation rate (SDR,  $\chi$ ), which characterises the rate of scalar mixing and can be evaluated from the spatial gradient of a scalar (Peters, 2000). Soulopoulos et al. (2015) measured the spatiotemporal evolution of the distributions of the mixture fraction and SDR in a starting turbulent jet within a quiescent environment using Planar Laser-induced fluorescence (PLIF) technique. Statistical analysis of the mixture fraction results revealed quick changes in the

mixing with radial distance around the shear layer and the passage of the vortex ring. It was also found that the probability density functions (PDFs) of the SDR had a universal characteristic shape at various locations in the flow and times after the start of injection (ASIs), which nevertheless differed from the usually suggested lognormal distribution. However, to the authors' knowledge, no such investigation in a turbulent environment has been reported to characterise the impact of the ambient turbulence on the mixing of starting turbulent jets.

The present study presents an experimental investigation on the mixing of a starting turbulent jet within different levels of background turbulence, which was homogeneous and isotropic. PLIF technique, combined with an advance imaging denoising method, was used to measure the mixture fraction fields at various ASIs, from which the SDR fields were also evaluated. The effect of ambient turbulence on the mixing of the starting jet was examined, which could be of significance to better understanding the combustion process of fuel jets in internal combustion engines.

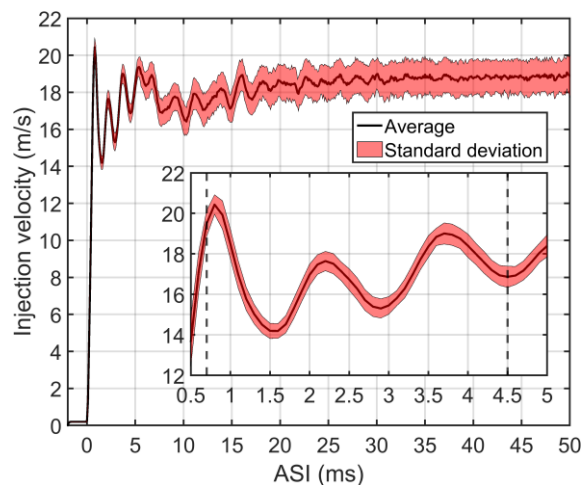
## 2. Experimental method

Figure. 1 shows schematically the experimental setup used in this study. The HIT environment was generated within a "box of turbulence" facility. The details of this facility have been reported in our previous publications (Charalampous & Hardalupas, 2010; Chen et al., 2018; Lian et al., 2017); therefore, only a brief description is provided here. The facility comprises a cubic aluminium frame, with an edge length of 1 m, and eight loudspeakers that are mounted on the vertices of the cube and pointed towards the centre of the cube. Each loudspeaker is capped with a perforated plate and driven individually by a 50-Hz sinusoidal voltage signal. The vibrating motion of each loudspeaker's membrane creates a synthetic jet array above the perforated plate, and the interaction of the four pairs of opposing jet arrays generates turbulence within the cubic frame. When the intensities of these jet arrays are balanced by tuning the amplitudes of the loudspeakers' driving signals, the turbulence in the region near the centre of the cubic frame becomes homogeneous and isotropic, and the mean velocity of the flow within this region remains close to zero. PIV measurements of the velocity fields showed that the HIT region has a dimension of approximately  $40 \times 40 \times 40 \text{ mm}^3$ . The intensity of the HIT can be controlled by the amplitudes of the loudspeakers' driving signals. The HIT considered in this study had a turbulent Reynolds number of 190 and 250, with the RMS velocity  $u'_{HIT} = 0.38$  and  $0.63 \text{ m/s}$ , and the Kolmogorov timescale  $\tau_k = 5.0$  and  $2.4 \text{ ms}$  respectively; the integral length scale for both levels of HIT were about 50 mm.



**Figure. 1** Schematic of the experimental setup for PLIF measurements of the starting jet

The starting turbulent jet of air was injected vertically upward into the HIT region via a straight tube, with an inner diameter of  $D = 4$  mm and wall thickness of 1 mm. The length-to-diameter ratio of the tube was 20, which ensured fully developed flow within the tube. The tube was positioned with its tip at the bottom centre of the HIT region to maximize the interaction of the ambient HIT with the starting jet. Pulsed injection was controlled by a solenoid valve (DM4, Keihin), with a response time of approximately 2.1 ms. Injection velocity, controllable via a needle valve (SS-4MG-MH, Swagelok), was measured at 1 mm downstream of the centre of the tube exit using Constant Temperature Anemometry with a sampling rate of 10 kHz, and the result is presented in Figure. 2. The injection velocity had a steady state value of  $U = 18.8$  m/s, corresponding to a Reynolds number of  $Re = 4800$  and a characteristic time scale of  $t^* = D/U = 0.21$  ms at the nozzle exit. Therefore, the starting turbulent jet of this study is very similar to that studied by Soulopoulos et al. (2015). However, large temporal variations in the injection velocity were observed during the initial stage of the starting jet.



**Figure. 2** Temporal evolution of the injection velocity for a 50-ms pulsed injection. The ensemble-averaged mean and standard deviation of the fluctuations of the velocity are evaluated from 125 pulsed injections. Vertical dashed lines in the inset plot mark the time window of PLIF measurements: ASI = 0.7 – 4.5 ms.

PLIF visualization and quantification of the jet mixing were realized by seeding the air jet with acetone vapour with a volume concentration of about 18% and exciting the acetone molecules with a frequency-quadrupled Nd:YAG laser (wavelength 266 nm, pulse duration 5 ns, pulse energy 19 mJ). Any residual 532-nm laser light was removed from the 266-nm laser beam using a Pellin Broca prism before the laser beam was shaped into a thin laser sheet and then passed through the centreline of the starting jet. The intensity of the emitted fluorescence was recorded using a CCD camera (Image Intense, LaVision), fitted with a Nikkor 50 mm f/1.4 lens and a close-up lens with a focal length of 500 mm. The camera sensor, with an original pixel array of 1376 x 1040, was 2 x 2 binned to increase the signal-to-noise ratio (SNR), resulting in a nominal resolution of 63  $\mu\text{m}/\text{pixel}$ . No image intensifier was used, thereby avoiding deterioration of the imaging system's optical resolution. The actual optical resolution of the imaging system was characterised with the scanning knife-edge technique (Clemens, 2002; Hua et al., 2021; Soulopoulos et al., 2014), and the measured line spread function indicated a FWHM (full width at half maximum) resolution of 66.57  $\mu\text{m}$ . The combination of the laser sheet height and the imaging system allowed for PLIF visualization of the jet mixing within an axial range of 0 – 10  $D$ . PLIF measurements were conducted at different times after the start of injection (ASI) within a time window of  $\text{ASI} = 0.7 - 4.5 \text{ ms}$ , or  $\text{ASI} = 3.3 - 21.4 t^*$ . For each ASI, 500 instantaneous PLIF images were collected, denoised with Wiener filters (Hua et al., 2021; Mulla & Hardalupas, 2022; Soulopoulos et al., 2014) and then processed to quantify the spatial distribution of jet fluid mixture fraction  $\xi$ . Scalar dissipation rate (SDR,  $\chi$ ) was evaluated following  $\chi = 2D[(\partial\xi/\partial x)^2 + (\partial\xi/\partial y)^2]$  with the gradient obtained through the central difference method and the molecular diffusivity taken as  $D = 10 \text{ mm}^2/\text{s}$  (Lugg, 1968; Yaws, 2009). Note that the  $xy$  coordinate system used here had its origin coinciding with the centre of the nozzle exit and its  $x$  and  $y$  axes propagating along the radial and axial directions of the jet respectively.

### 3. Results and discussion

#### 3.1 Instantaneous mixture fraction field and jet penetration length

Figure. 3 presents sample instantaneous spatial distributions of the mixture fraction in the starting jet within different levels of ambient HIT for  $\text{ASI} = 3.3, 7.6, 11.9$  and  $16.7 t^*$ . The leading vortex ring at the front of the jet – a characteristic feature of starting jets that is due to the roll up of the jet shear layer (Krueger & Gharib, 2003) – can be distinctly identified at the edge of the jet at the early stages, e.g.,  $\text{ASI} = 3.3 t^*$ , for all levels of ambient HIT. The entrainment of ambient fluid by the leading vortex ring is indicated by the low mixture fraction near the core of the vortex. Closer

examination of the mixture fraction distributions at  $ASI = 3.3 t^*$  reveals that an increasing portion of ambient fluids was present within the vortex ring when the ambient HIT became stronger, indicating that the ambient HIT was able to affect the entrainment of ambient fluids by the vortex ring at such an early stage although the ASI was much smaller than the Kolmogorov timescales of the ambient HIT.

As the jet developed, the leading vortex ring moved downstream with its size growing rapidly from about  $0.5 D$  in diameter at  $ASI = 3.3 t^*$  to about  $1 D$  at  $ASI = 7.6 t^*$  but remaining relatively unchanged afterwards. A trailing jet was formed between the leading vortex ring and the nozzle exit. From  $ASI = 3.3 t^*$  to  $7.6 t^*$ , the leading vortex ring gradually penetrated towards the jet axis by entraining the jet fluids near the axis, as evidenced by the shrinking of the jet stem surrounded by the leading vortex ring and by the fact that the mixture fraction within the vortex ring remained high. This agrees with the observation by Iglesias et al. (2005) that the leading vortex ring mainly entrained jet fluids instead of ambient fluids up to at least  $ASI = 25 t^*$ . As the leading vortex ring entrained jet fluids, it also gradually became disconnected from the trailing jet, as demonstrated in Figure. 3 by the distributions at  $ASI = 11.9 t^*$  for three levels of ambient HIT. This process is known as the “pinch-off” of the leading vortex ring, which is believed to occur after the leading vortex ring has attained its maximum circulation and energy (Gao & Yu, 2010; Gharib et al., 1998). As the leading vortex ring moved away from the nozzle, the shear layer of the trailing jet continued to produce more vortex rings, as shown in Figure. 3 at  $ASI \geq 7.6 t^*$  for all three levels of ambient HIT. Adjacent trailing vortex rings could interact via a process called “leapfrogging” as they developed (Cheng et al., 2015; Wang et al., 2019; Yu et al., 2008). Leapfrogging occurs because the velocity induced by the front vortex ring causes the rear one to contract and accelerate in the streamwise direction, and concurrently, the velocity induced by the rear vortex ring causes the front one to expand and decelerate. Consequently, the rear vortex ring – in an ideal leapfrogging process – would penetrate through the front vortex ring, and this process will repeat (Cheng et al., 2015). In actual starting jets, however, the rear vortex ring often cannot penetrate through the front one due to the viscosity but instead catches up and merges with the front vortex ring, as observed by e.g., Yu et al. (2008) and Wang et al. (2019). This “unsuccessful” leapfrogging or merging process was also observed in the present study: for example, the complex structure within  $y = 3 - 5 D$  at  $ASI = 16.7 t^*$  for three levels of ambient HIT were due to the merging of the first and second vortex rings in the trailing jet.

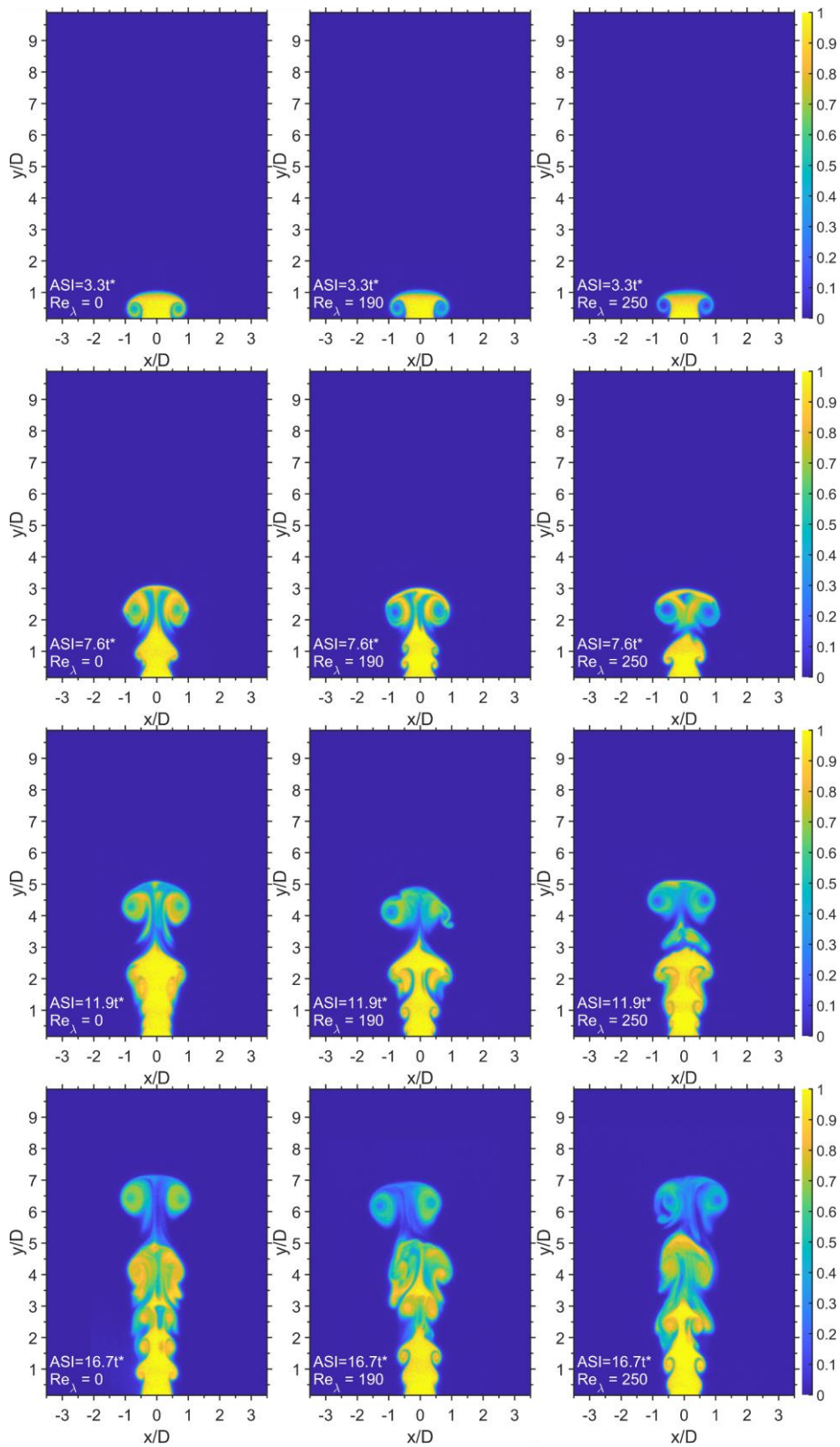
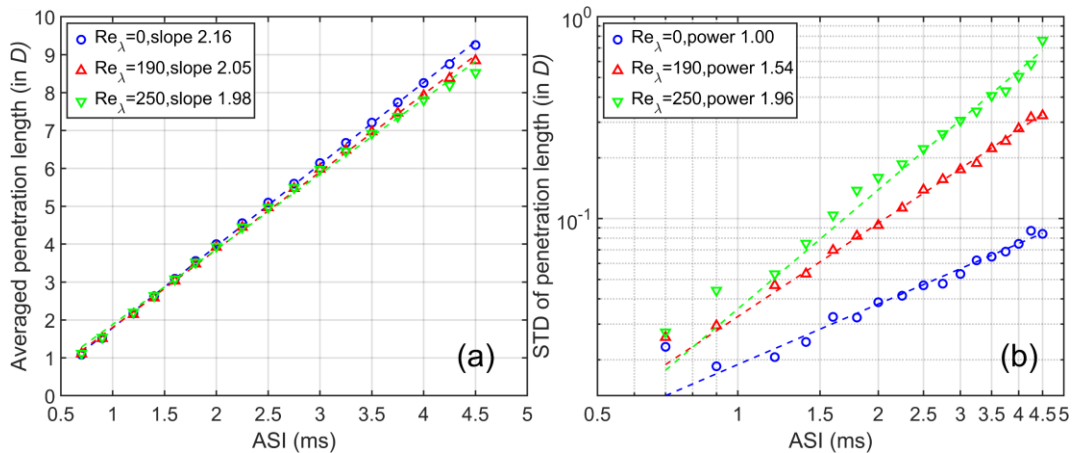


Figure. 3 Sample instantaneous planar distributions of mixture fraction at various ASIs and levels of HIT

It is also noted in Figure. 3 that both the leading vortex ring and the trailing vortex rings maintained a high degree of symmetry about the jet axis throughout the time window examined when the starting jet developed with no ambient HIT. Although the ambient HIT did not affect the symmetry of the leading vortex ring at the initial stage of its formation, e.g.,  $ASI = 3.3 t^*$ , it was able to deform the leading vortex ring at later stages. For example, strong deformation of the leading vortex ring by the ambient HIT can be observed for  $ASI = 11.9 t^*$  for  $Re_\lambda = 190$  and  $ASI = 16.7 t^*$  for  $Re_\lambda = 250$  in Figure. 3. In addition, the leading vortex ring at  $ASI = 16.7 t^*$  for  $Re_\lambda = 190$  appears tilted by the ambient HIT. The symmetry of the trailing vortex rings could be affected by the ambient HIT from the initial stage of their formation: for example, the first trailing vortex rings at  $ASI = 7.6 t^*$  for both  $Re_\lambda = 190$  and  $250$  appears slightly deformed. In addition, the trailing vortex rings also appear strongly deformed by the ambient HIT, e.g., at  $ASI = 16.7 t^*$ . Again, it is worth noting that the ASIs examined here are comparable to the Kolmogorov timescales of the ambient HIT.



**Figure. 4** Temporal evolution of the (a) ensemble average and (b) standard deviation of the penetration length of the starting jet with various levels of HIT. Note that the axes in (b) are presented in logarithmic scale. Dashed lines represent linear fits  $y = ax + b$  in (a) and power law fits  $y = ax^b$  in (b). Results of the fitted slopes and powers are included in the legends.

The penetration length of the starting jet was evaluated from each instantaneous planar distribution of mixture fraction with a threshold value of  $\xi = 0.05$ , and the ensemble average and standard deviation of the penetration length for each ASI are presented in Figure. 4. It has been reported, in both experimental and theoretical studies, that the penetration of a starting jet, without any ambient turbulence, correlates linearly with ASI in the near field but with the square root of ASI in the far field (Bajpai & Tirumkudulu, 2008; Inanc et al., 2016; Joshi & Schreiber, 2006; Witze, 1980). This transition of correlation is predicted to occur at a penetration length of  $7D$ , following the theory proposed by Witze (1980). However, it is also reported that the linear

correlation with ASI was maintained up to about  $20D$  (Cossali et al., 2001) and that the linear correlation with the square root of ASI was attained only beyond about  $30D$  (Bajpai & Tirumkudulu, 2008). The linear correlation with ASI for  $Re_\lambda = 0$  was observed here, as shown in Figure. 4(a), at least up to about  $9D$ . The penetration speed of the jet is evaluated to be 8.64 m/s for  $Re_\lambda = 0$  from the slope of the linear fit, which is about half of the injection velocity at the nozzle exit and in close agreement with the value reported by Soulopoulos et al. (2015). The standard deviation of the penetration length grew with ASI, as shown in Figure. 4(b), which is expected due to the development of turbulence within the jet; it is noted that the growth approximately follows a power law with regard to ASI.

The presence of ambient HIT introduced only marginal reductions in the averaged penetration length of the starting jet within the time window examined here: the maximum reduction was  $0.4D$  and  $0.7D$  at  $ASI = 4.5$  ms for  $Re_\lambda = 190$  and  $250$  respectively. In addition, the linear correlation between the penetration length and the ASI was not affected by the ambient HIT, as illustrated by the linear fits in Figure. 4(a). Nevertheless, the penetration speed saw a reduction to 8.21 and 7.93 m/s, i.e., a reduction of 5% and 8%, for  $Re_\lambda = 190$  and  $250$  respectively. The standard deviation of the penetration length, on the other hand, was substantially increased by the ambient HIT, as shown in Figure. 4(b): the increase, in comparison with  $Re_\lambda = 0$ , reached more than 3 times and 5 times after  $ASI = 2.5$  ms for  $Re_\lambda = 190$  and  $250$  respectively. It is surprising that the ambient HIT was able to impose such a strong impact on the location of the leading vortex ring within a window of ASI that was comparable to the Kolmogorov timescale of the ambient HIT. The standard deviation of the penetration length still grew with ASI following a power law even in the presence of the ambient HIT, but the growth rate was also substantially promoted by the ambient HIT, as shown by the power values of the data fits listed in Figure. 4(b). It is also worth noting that both the jet penetration speed and the power of the standard deviation of the penetration length increasing with ASI show a *linear* correlation with the RMS velocity of the ambient HIT.

### 3.2 Statistics of mixture fraction

The ensemble average of the mixture fraction and the standard deviation of the mixture fraction fluctuations were evaluated from the instantaneous mixture fraction distributions, and the results are presented in Figure. 5 and Figure. 6 respectively for  $ASI = 3.3, 7.6, 11.9$  and  $16.7 t^*$  with three levels of ambient HIT. The white dashed lines in Figure. 5 mark the axial location of the maximum width of the leading vortex ring, as an approximation of the axial location of the core of the leading vortex ring.

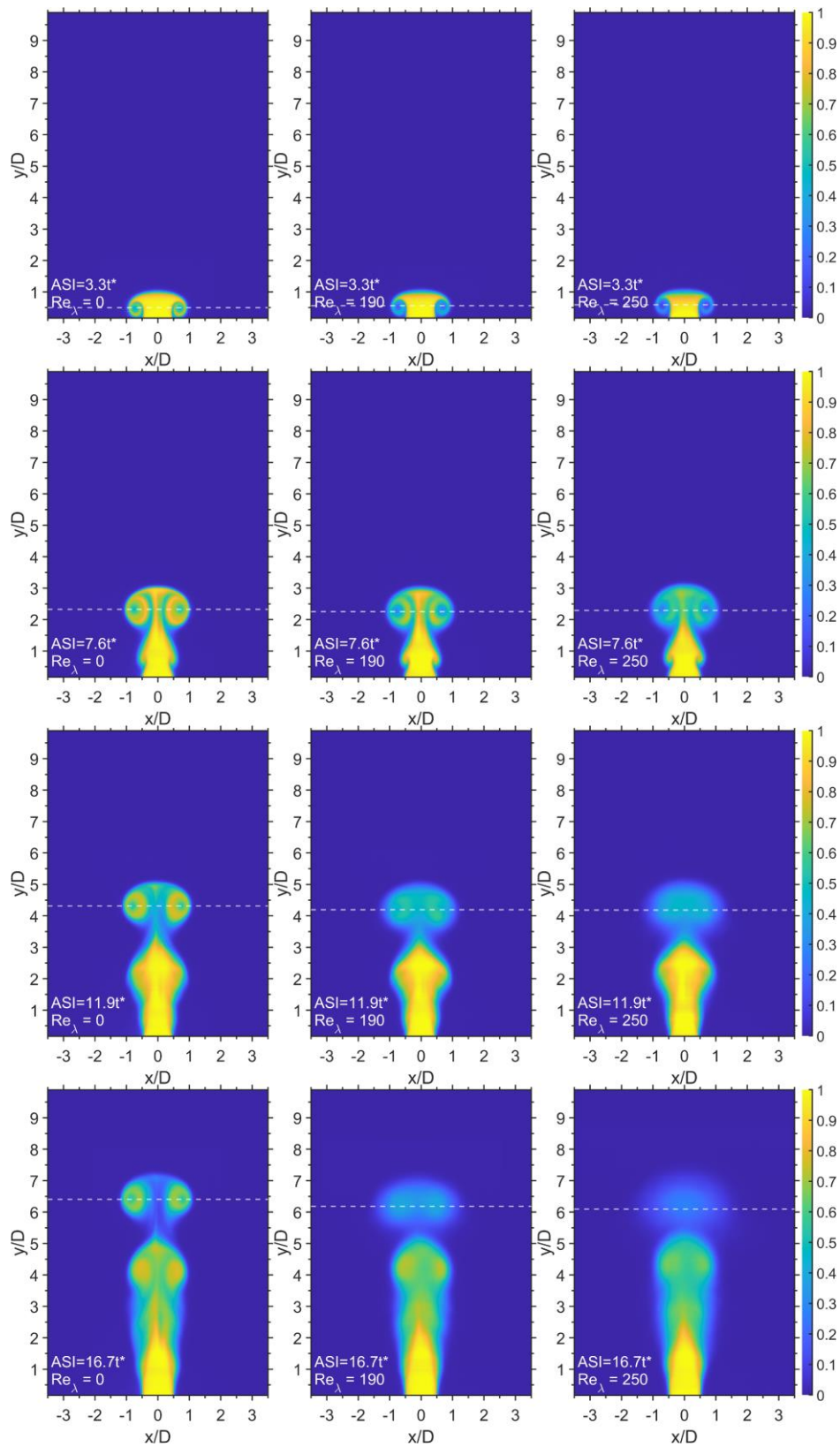


**Figure. 5** Ensemble-averaged planar distributions of mixture fraction at various ASIs and levels of HIT. The white dashed lines mark the axial location of the maximum width of the leading vortex ring, as an approximation of the axial location of the core of the leading vortex ring.

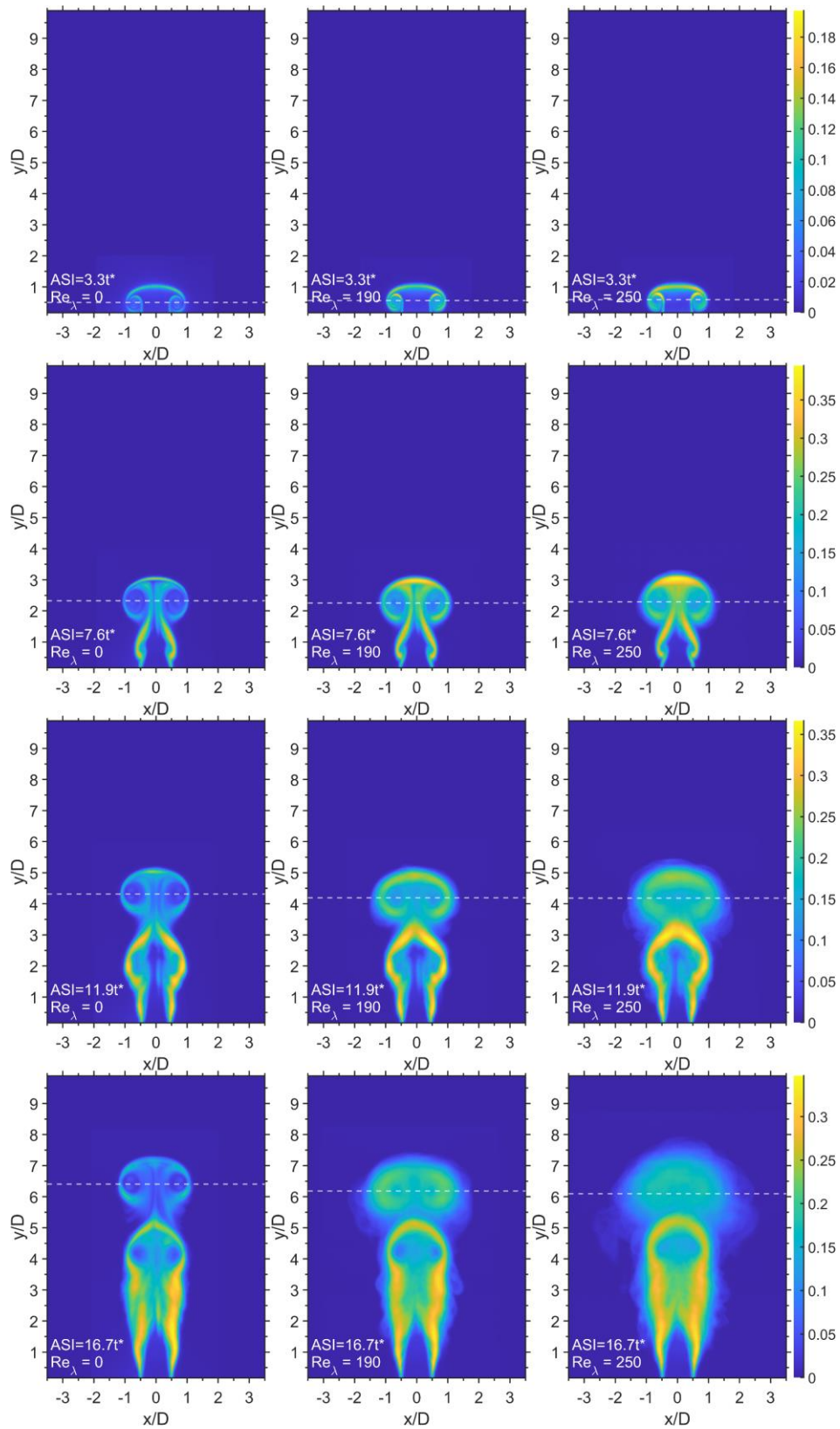


**Figure. 6** Planar distributions of standard deviation of mixture fraction fluctuations at various ASIs and levels of HIT.

Note that the colour scale is the same for three levels of HIT at an ASI.

It is found in Figure. 5 that there existed a “potential core”, i.e., a volume of pure jet fluids attached to the nozzle exit, in the starting jet, regardless of the presence of ambient HIT. Unlike the steady turbulent jets where the potential core has a conical shape and covers a certain axial range (typically  $y = 0 - 6 D$ ) (Lee & Chu, 2003; Mathieu & Scott, 2000), both the shape and the axial range of the potential core in the starting jets were found to vary with ASI. Moreover, this variation was closely related to the formation and evolution of the vortex rings. For example, the significant change in the potential core shape from  $ASI = 3.3 t^*$  to  $ASI = 7.6 t^*$  was caused by the expansion of the leading vortex ring and the formation of the trailing vortex rings. In addition, the axial range of the potential core shortened from about  $y = 0 - 3 D$  at  $ASI = 11.9 t^*$  to about  $y = 0 - 2 D$  at  $ASI = 16.7 t^*$  as the vortex rings formed in the trailing jet developed to gradually reach the jet centreline. It is also noted that no significant impact was introduced by the ambient HIT on either the shape or the axial range of the potential core in the starting jet.

The ensemble-averaged distributions of the mixture fraction at  $ASI = 3.3 t^*$  (top row in Figure. 5) confirms the observation from sample instantaneous mixture fraction distributions (see Figure. 3) that the ambient HIT was able to increase the amount of ambient fluids entrained by the vortex ring in the initial stage of its formation. To demonstrate this effect of ambient HIT more quantitatively, radial profiles of the mixture fraction along a line crossing the core of the leading vortex ring were extracted from Figure. 5 and plotted in Figure. 7(a). It is noted in Figure. 7(a) that the vortex ring straddled the radial range of  $|x| = 0.5 - 1 D$  for all three levels of ambient HIT, indicating that the location and size of the leading vortex ring in the early stages of its formation were not affected by the presence of ambient HIT. The peaks and valleys in Figure. 7(a) within the vortex ring regions are due to the layers of jet fluids and ambient fluids respectively that were rolled up during the formation of the vortex ring. The fact that the mixture fractions associated with the peaks were lower than 1 and those associated with the valleys were greater than 0 could be caused by (i) molecular mixing between the layer of jet fluids and the layer of ambient fluids, and (ii) fluctuations in the thickness and location of these layers, as demonstrated by the standard deviation results (see the top row of Figure. 6). The mixture fraction within the vortex ring region – including the peaks and valleys – reduced as the ambient HIT was increased, confirming the enhanced entrainment of ambient fluids into the vortex ring.

It is also noted in Figure. 5 that when the starting jet developed with no ambient HIT, there remained a small volume of relatively low mixture fraction around the core of the leading vortex ring throughout the time window examined. In addition, the radial location of this low mixture fraction region – and hence of the core of the leading vortex ring – remained approximately constant at  $x \approx 0.75 D$ , as shown by the radial profiles of the mixture fraction in Figure. 7.

Nevertheless, the mixture fraction within this region still increased with ASI: for example, the minimum mixture fraction within this region increased from  $\bar{\xi} = 0.4$  at  $ASI = 3.3 t^*$  to  $\bar{\xi} = 0.55$  at  $ASI = 16.7 t^*$ , as shown in Figure. 7; this increase in mixture fraction indicates the occurrence of molecular mixing. In the presence of ambient HIT, the small volume of relatively low mixture fraction around the vortex ring core remained observable in the ensemble-averaged mixture fraction fields until about  $ASI = 10.7 t^*$  and  $8.6 t^*$  for  $Re_\lambda = 190$  and  $250$  respectively. Its disappearance at later stages of the jet development within ambient HIT could be caused by the strong fluctuations in the instantaneous shape and position of the leading vortex ring imposed by the ambient HIT, as demonstrated in Figure. 3 as well as in Figure. 6. These fluctuations also explain the observation in Fig. 5 that the definition of the leading vortex ring in the ensemble-averaged mixture fraction fields becomes increasingly blurred with ASI in the presence of ambient HIT, and the blurredness increases with  $Re_\lambda$  for a certain ASI. Another consequence of these fluctuations is that the ensemble-averaged mixture fraction within the leading vortex ring reduced significantly when the ambient HIT was increased (e.g., see the results for  $ASI = 16.7 t^*$  in Figure. 5 and Figure. 7), indicating the effect of ambient HIT enhancing the mixing in the leading vortex ring. Increased blurredness in the definition of the first trailing vortex ring within ambient HIT was also observed for at  $ASI = 16.7 t^*$  in Fig. 5, but to a much lower degree compared to the leading vortex ring; however, the blurredness also became substantial at a later stage, e.g.,  $ASI = 21.4 t^*$  (mixture fraction distributions not shown here for brevity). Therefore, the main reason for the delayed blurring of the trailing vortex rings was their delayed formation in comparison to the leading vortex ring.

It is interesting to note in Figure. 7 that the radial profiles of the ensemble-averaged mixture fraction along the line crossing the core of the leading vortex ring have a Gaussian shape after  $ASI = 16.7 t^*$  for  $Re_\lambda = 250$ , while Gaussian-shaped radial profiles of mixture fraction is a characteristic of steady turbulent jets in the fully developed region (Lee & Chu, 2003). Although the Gaussian shape was not attained for the radial profiles for  $Re_\lambda = 190$  by  $ASI = 21.4 t^*$ , it was expected to take place at a later stage following the trend observed in Figure. 7. On the other hand, there is no clear sign of the radial profiles for  $Re_\lambda = 0$  approaching a Gaussian shape within the time window examined. These observations suggest that the presence of ambient HIT might be able to accelerate the transition of starting turbulent jets to steady turbulent jets.

Figure. 6 shows that in the initial formation stage of the leading vortex ring, i.e.,  $ASI = 3.3 t^*$ , large fluctuations of mixture fraction were concentrated at the leading edge of the jet and at the edge of the vortex ring, regardless of the level of the ambient HIT. Similar observations have been reported by Soulopoulos et al. (2015) for  $Re_\lambda = 0$ . As the leading vortex ring moved downstream

from the nozzle exit and the trailing jet established, additional large fluctuations in the mixture fraction started to appear in the trailing jet, first in the shear layer of the trailing jet and later also at the edge of the trailing vortex rings. The magnitude of the fluctuations in the trailing jet was first comparable to – but quickly exceeded – that in the leading vortex ring. It is also found that the maximum standard deviation of the fluctuations within the jet increased rapidly with ASI in the early stage (up to about  $ASI = 7.5 t^*$ ) but remained relatively constant at about  $\xi' = 0.35$  until the maximum examined  $ASI = 21.4 t^*$ , regardless of level of the ambient HIT.

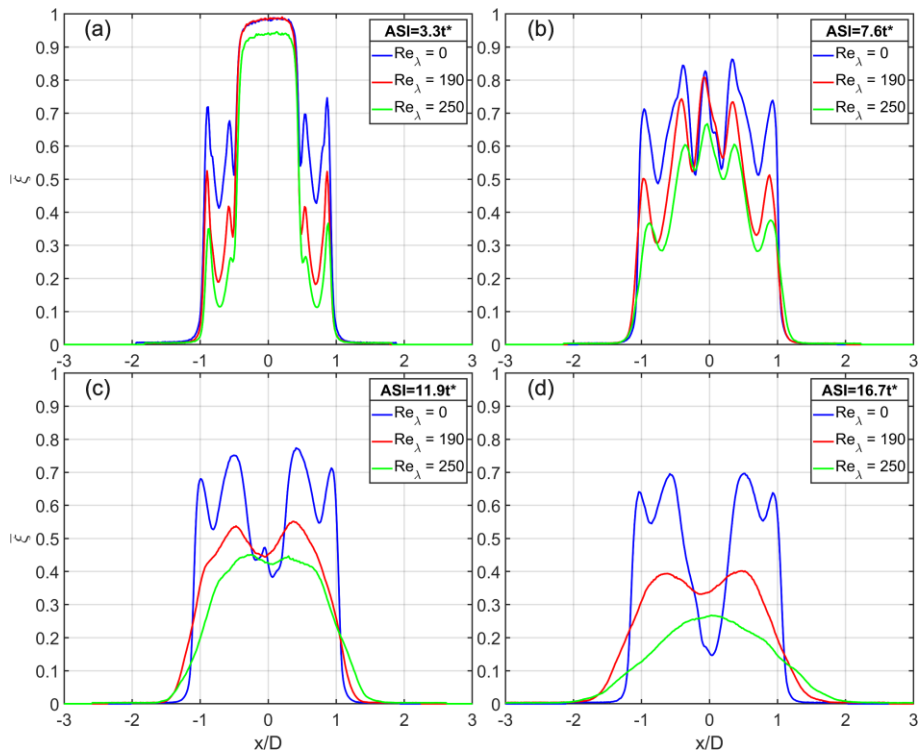


**Figure. 7** Radial variation of ensemble averaged mixture fraction along the line crossing the core of the leading vortex ring for various ASIs and levels of HIT. Axial locations of the lines are demonstrated in Figure. 5.

Ambient turbulence was able to enhance the fluctuations of mixture fraction, particularly in the region of the leading vortex ring. To demonstrate this more quantitatively, radial variations of the standard deviation along the line crossing the core of the leading vortex ring are plotted in Figure. 8. In comparison to the case with  $Re_\lambda = 0$ , the standard deviation within the leading vortex ring increased substantially when ambient HIT was introduced, even in the very early stage of the starting jet when the ASI was much smaller than the Kolmogorov timescale of the ambient HIT. At  $ASI = 3.3 t^*$ , for example, the standard deviation at about  $|x| = 0.7 D$  (i.e., the core the vortex ring) was increased from about 0.04 for  $Re_\lambda = 0$  to about 0.07 when ambient HIT was introduced. Figure. 6 shows a less significant impact of the ambient HIT on the fluctuations in the region of the trailing

vortex rings compared with the leading vortex ring, similar to the observation about the impact of ambient HIT on the distributions of ensemble-averaged mixture fraction in Figure. 5; this, again, could be explained by the delayed formation of the trailing vortex rings.

It is interesting to note that the fluctuations of mixture fraction remained low ( $\xi' \approx 0.04$ ) around the core the leading vortex ring as the jet developed with no ambient HIT. Considering that the mixture fraction in the same region gradually increased with ASI when  $Re_\lambda = 0$ , as shown in Figure. 5 and Figure. 7, it is concluded that despite the strong circulating motion of the leading vortex ring, the mixing in the region near its core – in the absence of ambient HIT – was dominated by molecular mixing. In the presence of ambient HIT, however, the initially distinct structures of the standard deviation in the region of the leading vortex ring quickly disappeared as the jet developed, e.g., see  $ASI = 11.9$  and  $16.7 t^*$  in Figure. 6, which was again due to the strong deformation and transportation of the leading vortex ring imposed by the ambient HIT, indicating the dominant role of turbulent mixing.

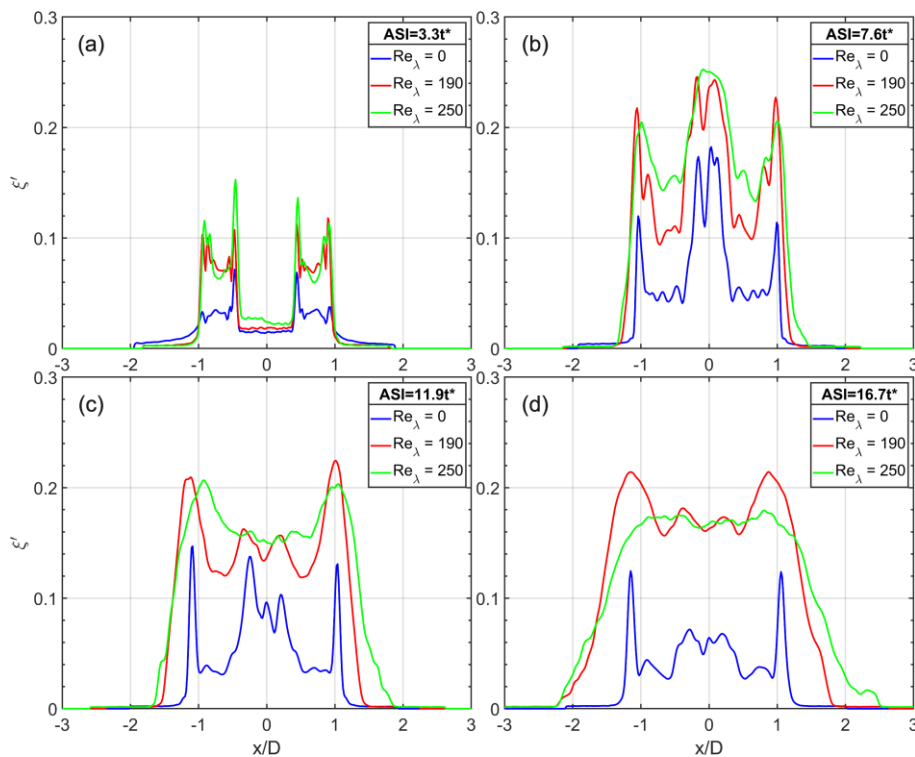


**Figure. 8** Radial variation of standard deviation of mixture fraction fluctuations along the line crossing the core of the leading vortex ring for various ASIs and levels of HIT. Axial locations of the lines are demonstrated in Figure. 6.

To quantify the overall mixing of the starting jet, PDFs of the ensemble-averaged mixture fraction were evaluated, and the results are presented in Figure. 9. The evaluation of the PDFs used the data from the region of the jet enclosed by the contour of  $\bar{\xi} = 0.05$ , ensuring the presence of jet fluids and thereby avoiding the bias of the PDF by the large amount of pure ambient fluids within the

field of view. At  $ASI = 3.3 t^*$ , all three PDFs show a distinct peak at  $\bar{\xi}$  close to 1, which is due to the large volume of the jet stem and the limited entrainment of ambient fluids by the vortex ring, as observed in Figure. 5. However, the height of this peak reduced as  $Re_\lambda$  increased, which was accompanied by an increase in the probability of  $\bar{\xi}$  being close to 0, e.g.,  $\bar{\xi} = 0.05 - 0.3$ ; this was attributed to the increased amount of ambient fluids entrained by the vortex ring, as discussed in the context of Figure. 5. The PDFs also show a noticeable probability of intermediate mixture fractions, e.g.,  $\bar{\xi} = 0.4 - 0.8$ : 35%, 23% and 21% for  $Re_\lambda = 0, 190$  and  $250$  respectively; this suggests that a noticeable amount of molecular mixing had occurred by  $ASI = 3.3 t^*$ .

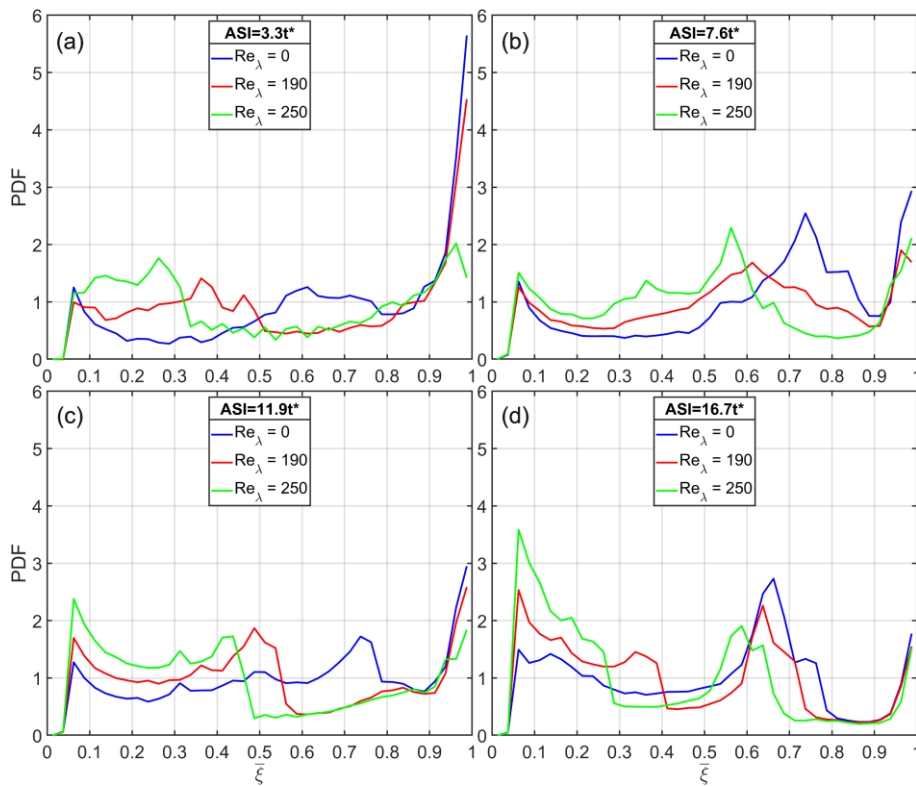


**Figure. 9** PDFs of ensemble averaged mixture fraction in the starting jet with various ASIs and levels of HIT. Each PDF is evaluated with a bin width of  $\Delta\bar{\xi} = 0.025$  using the pixels enclosed by the contour of  $\bar{\xi} = 0.05$ .

Compared to the PDFs at  $ASI = 3.3 t^*$ , those at  $ASI = 7.6 t^*$  show a reduced probability for both the low values (e.g.,  $\bar{\xi} < 0.3$ ) and high values (e.g.,  $\bar{\xi} > 0.8$ ) of the mixture fraction. At the same time, the probability of intermediate mixture fraction increased for all three levels of ambient HIT; distinct peaks at  $\bar{\xi} = 0.73, 0.61$  and  $0.57$  can be found for  $Re_\lambda = 0, 190$  and  $250$  respectively. As observed in Figure. 5, these intermediate mixture fractions were mainly distributed within the leading vortex ring and the shear layer of the trailing jet. Therefore, the changes in the PDFs could be explained by (i) the further mixing of the jet fluids with the entrained ambient fluids in the leading vortex ring, and (ii) the increased volume of the shear layer as the jet grows.

As the jet developed to  $ASI = 11.9 t^*$ , the peak at  $\bar{\xi} \approx 0.75$  observed at  $ASI = 7.6 t^*$  in the PDF for  $Re_\lambda = 0$  had seen a significant reduction, accompanied by an increase in the probability of lower mixture fractions, e.g.,  $\bar{\xi} < 0.5$ . This is because, as shown in Figure. 5, the leading vortex ring was in the process of pinching off from the trailing jet at  $ASI = 11.9 t^*$  for  $Re_\lambda = 0$ , producing a large volume of low mixture fractions within the jet stem connecting the leading vortex ring and the trailing jet. Further development of the pinch-off of the leading vortex ring led to a further increase in the probability of low mixture fractions, as shown in the PDF for  $Re_\lambda = 0$  at  $ASI = 16.7 t^*$ . More significant increase in the probability of low mixture fractions after  $ASI = 7.6 t^*$  was observed in Figure. 9 when the level of ambient HIT was increased, which was mainly due to the enhanced mixing within the leading vortex ring by the ambient turbulence, as shown in Figure. 5.

The vortex rings in the trailing jet had also entrained some ambient fluids by at  $ASI = 11.9 t^*$  (see Figure. 5), but these trailing rings were still dominated by jet fluids with high mixture fractions and therefore had little contribution to the increased probability of low mixture fractions in the PDFs. Nevertheless, the further development of – and the mixing within – these trailing vortex rings led to a large volume of fluids with  $\bar{\xi} \approx 0.6 - 0.7$  within the axial range of  $y = 2 - 5 D$  at  $ASI = 16.7 t^*$ , as shown in Figure. 5, which explains the appearance of an increased peak at  $\bar{\xi} = 0.6 - 0.7$  in the PDFs at  $ASI = 16.7 t^*$  (see Figure. 9(d)). This peak appeared at a reduced level of mixture fraction when the ambient HIT was increased, indicating an impact of enhancing the mixing within the trailing vortex rings by the ambient HIT.

### 3.3 Scalar dissipation rate

Figure. 10 presents the distributions of the natural logarithm of the ensemble averaged SDR, i.e.,  $\ln(\bar{\chi})$  at  $ASI = 3.3, 7.6, 11.9$  and  $16.7 t^*$  for three levels of ambient HIT. These distributions have a similar appearance to those of the standard deviation of the mixture fraction fluctuations shown in Figure. 6. In the absence of ambient HIT, the high SDR regions formed a layer that coincides with the leading edge of the starting jet and with the edge of the leading vortex ring when the leading vortex ring was still attached to the nozzle exit, i.e.,  $ASI = 3.3 t^*$ . This is in agreement with the experimental results reported by Soulopoulos et al. (2015) and the computational results reported by Inanc et al. (2016) for the same stage of the starting jet development. However, the present measurements also showed some thin layers of intermediate SDR within the leading vortex ring, which was absent in the results by Soulopoulos et al. (2015); this indicates the advantages of the improved resolution of the imaging system used here.

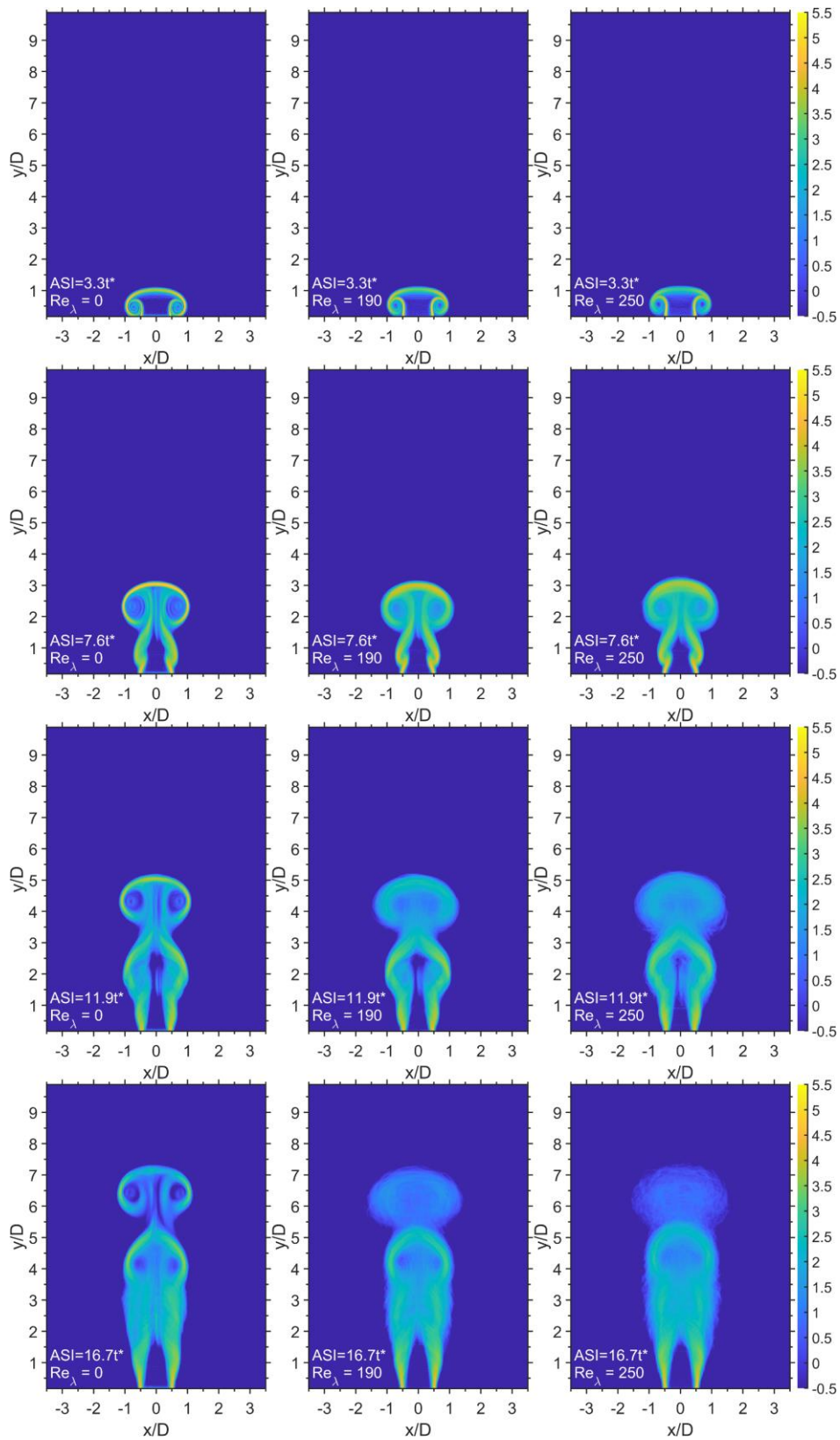


Figure. 10 Planar distribution of the natural logarithm of ensemble averaged SDR  $\ln(\bar{\chi})$  at various ASIs and levels of

HIT

Because the following development of the leading vortex ring mainly entrained jet fluids from the jet stem, as discussed in the context of Figure. 3, the SDR around the core of the leading vortex ring was much lower than that along the edge of the ring, as observed for  $Re_\lambda = 0$  in Figure. 10. In addition, there is a trend for the SDR around the core of the leading vortex ring to gradually reduce with ASI, which was because of the molecular mixing constantly lowering the mixture fraction gradient. High SDR regions in the trailing jet were mainly distributed along the shear layer before the formation of the trailing vortex rings, after which they were gradually expanded to reach the jet centreline by the development of the trailing vortex rings, as shown in Figure. 10 for  $ASI = 16.7 t^*$  and  $Re_\lambda = 0$ . Within the axial range of the shear layer of the trailing jet, however, the high SDRs remained in a layer along the shear layer; the thickness of the layer grew with the axial distance from the nozzle following that of the shear layer.

The presence of ambient HIT introduced no distinct changes to the distribution of high SDRs within the starting jet in the initial formation stage of the leading vortex ring, as shown in the top row of Figure. 10. As the leading vortex ring evolved and got deformed/transported by the ambient HIT, the high SDRs gradually became uniform distributed in the region of the leading vortex ring instead of being concentrated along the edge of the ring; consequently, the maximum SDR in the region of the leading vortex ring gradually approached a negative correlation with the level of ambient HIT, as can be seen from the results for  $ASI = 16.7 t^*$  in Figure. 10. Similar impact was observed for the SDRs in the region of the trailing vortex rings. On the other hand, the ambient HIT showed no noticeable impact on either the distribution or the magnitude of the SDRs in the region of the shear layer close to the nozzle exit.

#### 4. Conclusions

The impact of ambient turbulence on the mixing of a starting turbulent jet was experimentally investigated within an environment of homogeneous and isotropic turbulence. The jet was injected through a straight tube with a length-to-diameter ratio of 20; the injection velocity of  $U = 18.8$  m/s and nozzle diameter of  $D = 4$ mm led to a Reynolds number of 4800 and a characteristic time scale of  $t^* = 0.21$  ms at the nozzle exit. Two levels of ambient HIT were examined with a turbulent Reynolds number of  $Re_\lambda = 190$  and 250 respectively. Spatial distributions of the mixture fraction and SDR were obtained at various ASIs within a time window of  $ASI = 3.3 - 21.4 t^*$  from PLIF measurements of the jet fluid concentration field. The main findings from this study are summarized as follows.

- (1) During the initial formation of the leading vortex ring, the ambient HIT was able to increase the amount of entrained ambient fluids while not altering the location and size of the vortex ring. At later stages, it caused strong deformation and transportation of the leading vortex ring, although the ASIs were only comparable to its Kolmogorov timescale.
- (2) The starting jet penetrated the ambient fluids with a constant speed within the time window examined, regardless of the level of ambient HIT. While the jet penetration speed decreased less than 10% in the presence of ambient HIT, the fluctuations in the jet penetration length increased substantially with the level of ambient HIT. Nevertheless, the standard deviation of the fluctuations always grew with ASI following a power law.
- (3) The ensemble-averaged mixture fraction within the leading vortex ring was significantly reduced, whereas the mixture fraction fluctuations were substantially increased, by the ambient HIT. Similar – but less considerable – impact of the ambient HIT was observed in the trailing vortex rings. PDFs of the ensemble averaged mixture fraction showed that the ambient HIT increased the probability of low mixture fractions, indicating an enhancement of the overall mixing of the starting jet.
- (4) Ensemble averaged SDR results showed concentrated distributions of high SDRs along the boundaries of the jet and the leading vortex ring in the initial formation stage of the leading vortex ring, regardless of the level of the ambient HIT. At later stages, while the high SDRs in the leading vortex ring remained concentrated along the vortex ring boundaries for  $Re_\lambda = 0$ , it became increasingly uniformly distributed with a lower maximum value as the ambient HIT increased. Less significant impact of the ambient HIT on the SDR fields was observed in the trailing vortex rings, while no noticeable impact was found in the shear layer close to the nozzle exit.

## Acknowledgements

The authors would like to acknowledge the financial support from the Engineering and Physical Science Research Council (EPSRC) through the Industrial Decarbonization Research and Innovation Centre (IDRIC, grant number EP/V027050/1), and from the Horizon Europe programme through the Highly Efficient Super Critical ZERO eMission Energy System (HERMES) project (grant number 101083748).

## References

- Bajpai, S., & Tirumkudulu, M. S. (2008). An experimental study of impulsively started turbulent axisymmetric jets. *The European Physical Journal B*, 61(3), 293–297. <https://doi.org/10.1140/epjb/e2008-00068-2>
- Charalampous, G., & Hardalupas, Y. (2010). Clustering of mono-disperse and poly-disperse particles in a “box of turbulence”. 7th International Conference on Multiphase Flow, Tampa, FL USA.
- Chen, C., Charalampous, G., Shi, Z., & Hardalupas, Y. (2018, July 16). Laser-induced spark ignition of pulsed methane jets in homogeneous and isotropic turbulence without mean flow. 19th International Symposium on the Application of Laser and Imaging Techniques to Fluid Mechanics. 19th International Symposium on the Application of Laser and Imaging Techniques to Fluid Mechanics, Lisbon, Portugal.
- Cheng, M., Lou, J., & Lim, T. T. (2015). Leapfrogging of multiple coaxial viscous vortex rings. *Physics of Fluids*, 27(3), 031702. <https://doi.org/10.1063/1.4915890>
- Clemens, N. T. (2002). Flow Imaging. In J. P. Hornak (Ed.), *Encyclopedia of Imaging Science and Technology*. <https://doi.org/10.1002/0471443395.img022>
- Cossali, G. E., Coghe, A., & Araneo, L. (2001). Near-Field Entrainment in an Impulsively Started Turbulent Gas Jet. *AIAA Journal*, 39(6), 1113–1122. <https://doi.org/10.2514/2.1424>
- Gao, L., & Yu, S. C. M. (2010). A model for the pinch-off process of the leading vortex ring in a starting jet. *Journal of Fluid Mechanics*, 656, 205–222. <https://doi.org/10.1017/S0022112010001138>
- Gaskin, S. J., McKernan, M., & Xue, F. (2004). The effect of background turbulence on jet entrainment: An experimental study of a plane jet in a shallow coflow. *Journal of Hydraulic Research*, 42(5), 533–542. <https://doi.org/10.1080/00221686.2004.9641222>
- Gharib, M., Rambod, E., & Shariff, K. (1998). A universal time scale for vortex ring formation. *Journal of Fluid Mechanics*, 360, 121–140. <https://doi.org/10.1017/S0022112097008410>
- Hua, X., Liu, Y., Chen, C., Hardalupas, Y., & Taylor, A. M. K. P. (2021). Mixing and scalar dissipation rate in a decaying jet. *Proceedings of the Combustion Institute*, 38(2), 3251–3259. <https://doi.org/10.1016/j.proci.2020.08.042>
- Iglesias, I., Vera, M., Sánchez, A. L., & Liñán, A. (2005). Simulations of starting gas jets at low Mach numbers. *Physics of Fluids*, 17(3), 038105. <https://doi.org/10.1063/1.1858533>
- Inanc, E., Nguyen, M. T., Kaiser, S., & Kempf, A. M. (2016). High-resolution LES of a starting jet. *Computers & Fluids*, 140, 435–449. <https://doi.org/10.1016/j.compfluid.2016.10.022>

- Johari, H., Zhang, Q., Rose, M. J., & Bourque, S. M. (1997). Impulsively Started Turbulent Jets. *AIAA Journal*, 35(4), 657–662. <https://doi.org/10.2514/2.186>
- Joshi, A., & Schreiber, W. (2006). An experimental examination of an impulsively started incompressible turbulent jet. *Experiments in Fluids*, 40(1), 156–160. <https://doi.org/10.1007/s00348-005-0058-9>
- Khorsandi, B., Gaskin, S., & Mydlarski, L. (2013). Effect of background turbulence on an axisymmetric turbulent jet. *Journal of Fluid Mechanics*, 736, 250–286. <https://doi.org/10.1017/jfm.2013.465>
- Krueger, P. S., & Gharib, M. (2003). The significance of vortex ring formation to the impulse and thrust of a starting jet. *Physics of Fluids*, 15(5), 1271–1281. <https://doi.org/10.1063/1.1564600>
- Lee, J. H. W., & Chu, V. H. (2003). Turbulent Jets. In *Turbulent Jets and Plumes: A Lagrangian Approach* (pp. 21–54). Springer US. [https://doi.org/10.1007/978-1-4615-0407-8\\_2](https://doi.org/10.1007/978-1-4615-0407-8_2)
- Lian, H., Soulopoulos, N., & Hardalupas, Y. (2017). Evaluation of the topological characteristics of the turbulent flow in a ‘box of turbulence’ through 2D time-resolved particle image velocimetry. *Experiments in Fluids*, 58(9). <https://doi.org/10.1007/s00348-017-2395-x>
- List, E. J. (1982). Turbulent Jets and Plumes. *Annual Review of Fluid Mechanics*, 14(1), 189–212. <https://doi.org/10.1146/annurev.fl.14.010182.001201>
- Lugg, G. A. (1968). Diffusion coefficients of some organic and other vapors in air. *Analytical Chemistry*, 40(7), 1072–1077. <https://doi.org/10.1021/ac60263a006>
- Mathieu, J., & Scott, J. (2000). *An Introduction to Turbulent Flow*. Cambridge University Press; Cambridge Core. <https://doi.org/10.1017/CBO9781316529850>
- Mulla, I. A., & Hardalupas, Y. (2022). Measurement of instantaneous fully 3D scalar dissipation rate in a turbulent swirling flow. *Experiments in Fluids*, 63(11), 173. <https://doi.org/10.1007/s00348-022-03518-2>
- Perez Alvarado, A. (2016). *Effect of background turbulence on the scalar field of a turbulent jet: Vol. PhD [PhD]*. McGill University.
- Peters, N. (2000). *Turbulent Combustion*. Cambridge University Press; Cambridge Core. <https://doi.org/10.1017/CBO9780511612701>
- Pope, S. B. (2000). *Turbulent Flows*. Cambridge University Press; Cambridge Core. <https://doi.org/10.1017/CBO9780511840531>
- Sahebjam, R., Kohan, K. F., & Gaskin, S. (2022). The dynamics of an axisymmetric turbulent jet in ambient turbulence interpreted from the passive scalar field statistics. *Physics of Fluids*, 34(1), 015129. <https://doi.org/10.1063/5.0071023>
- Soulopoulos, N., Hardalupas, Y., & Taylor, A. M. K. P. (2014). Scalar dissipation rate measurements in a starting jet. *Experiments in Fluids*, 55(3). <https://doi.org/10.1007/s00348-014-1685-9>

- Soulopoulos, N., Hardalupas, Y., & Taylor, A. M. K. P. (2015). Mixing and scalar dissipation rate statistics in a starting gas jet. *Physics of Fluids*, 27(12), 125103. <https://doi.org/10.1063/1.4935233>
- Tennekes, H., & Lumley, J. L. (1972). *A first course in turbulence*. MIT Press.
- Wang, X. K., Su, B. Y., Li, Y. L., & Wang, C. (2019). Vortex formation and evolution process in an impulsively starting jet from long pipe. *Ocean Engineering*, 176, 134–143. <https://doi.org/10.1016/j.oceaneng.2019.02.041>
- Witze, P. O. (1980). The Impulsively started incompressible turbulent jet (SAND-80-8617). Sandia National Laboratories. <https://www.osti.gov/servlets/purl/5017517>
- Yaws, C. L. (2009). Chapter 10—Diffusion Coefficient in Air – Organic Compounds. In C. L. Yaws (Ed.), *Transport Properties of Chemicals and Hydrocarbons* (pp. 407–496). William Andrew Publishing. <https://doi.org/10.1016/B978-0-8155-2039-9.50015-6>
- Yu, S. C. M., Ai, J. J., Gao, L., & Law, A. W. K. (2008). Vortex Formation Process of a Starting Square Jet. *AIAA Journal*, 46(1), 223–231. <https://doi.org/10.2514/1.29514>
- Yu, S. C. M., Law, A. W.-K., & Ai, J. J. (2007). Vortex formation process in gravity-driven starting jets. *Experiments in Fluids*, 42(5), 783–797. <https://doi.org/10.1007/s00348-007-0290-6>